Primitive Chain Network Simulations of Probe Rheology

Yuichi Masubuchi[1]*, Yoshifumi Amamoto[1], Ankita Pandey[1] and Cheng-Yang Liu[2]

1 Department of Materials Physics, Nagoya University, Japan

2 Institute of Chemistry, Chinese Academy of Science, China

*Corresponding Author

E-mail: mas@mp.pse.nagoya-u.ac.jp; Tel +81-51-789-2551 (Y.M.).

ABSTRACT

The probe rheology experiments, in which the dynamics of a small amount of probe chains dissolved in immobile matrix chains is discussed, have been performed for the development of molecular theories for entangled polymer dynamics. Although the probe chain dynamics in the probe rheology is considered hypothetically as the single chain dynamics in the fixed tube-shaped confinement, it has not been fully elucidated. For instance, the end-to-end relaxation of probe chains is in retard of that for monodisperse melts, unlike the conventional molecular theories. In this study, viscoelastic and dielectric relaxations of probe chains were calculated by primitive chain network simulations. The simulations semi-quantitatively reproduced the dielectric relaxation, which reflects the effect of constraint release on the end-to-end relaxation. Fair agreement was also obtained for the viscoelastic relaxation time. However, the viscoelastic relaxation intensity was underestimated, possibly due to some flaws of the model for the inter-chain cross-correlations between probe and matrix chains.

Keywords: constraint release, entangled polymers, multi-chain slip-link simulations

1 Introduction

In spite of lots of attempts, description of polymer dynamics in entangled states is still a challenge[1,2]. Due to the significance in the polymer processing industry, polymer rheology has been one of the important issues in polymer science. Experimental attempts have revealed that the polymer rheology is compatible with the polymer dynamics (owing to the stress-optical rule[3]), and that the rheological behaviors of polymers with different chemistries are mostly universal[4]. On the basis of these findings, theoretical attempts for the description of polymer rheology with simplified molecular models have been performed, with embedding the effects of chemistries via inter-molecular interactions into a few model parameters. Such theoretical studies are based on the Rouse model[5], in which the polymer chain is represented by consecutive beads and springs, and no inter-bears interaction is considered. The Rouse model can reproduce linear viscoelasticity of polymer melts given that the molecular weight of polymers is relatively small and the polymer concentration is sufficiently high. On the other hand, the model fails for long polymers, for which the molecular weight is larger than a chemistry-dependent critical value. For such polymers, the dynamics is in retard

of the Rouse behavior. Because the mechanism of this retardation has been considered as the entanglement between polymers, the polymeric liquids with such behaviors are so-called entangled polymers[4].

Although the molecular detail of entanglement phenomena is still a matter of discussion, it has been rather established that the dynamics of entangled polymers can be cast into the dynamics of single polymer chain in a tube shape confinement[6,7]. In this framework, the polymer dynamics is decomposed into the test chain dynamics in the fixed tube and the tube dynamics so-called constraint release (CR) due to the motion of surrounding chains[1,8]. The former has been almost established in the recent molecular theories[9,10] that incorporate the reptation[7,11] and the contour length fluctuations (CLF)[12]. On the other hand, the CR dynamics is still a matter of investigation due to complicated multi-chain effects, although there have been established a few implementations of CR termed as Rouse-CR[13], double reptation[14,15] and dynamic tube dilation[16].

Effects of CR on polymer dynamics have been discussed in binary blends of polymers with well-separated molecular weights[17]. In particular, the experiments with a small amount of short chains dissolved in long chain matrices are so-called probe

rheology[18]. On the basis of the assumption in which the dynamics of short chains corresponds to the test chain dynamics without CR, results in probe rheology have been discussed in comparison to the dynamics of monodisperse melts[18].

Although polymer dynamics confined in an immobile tube constraint has been theoretically established, there have been reported a few unsolved issues. For instance, Matsumiya et al.[19] reported an interesting probe rheology study, in which they performed dielectric measurements of polyisoprene in addition to the viscoelastic measurements. Because polyisoprenes have type-A dipoles, the dielectric relaxation corresponds to the end-to-end relaxation of the molecule, whereas the viscoelastic relaxation conforms to the segment orientational relaxation. For the first time, they clearly demonstrated that the viscoelastic relaxation coincides with the dielectric relaxation for the probe chain. This result supports the tube framework, in which the segment orientational relaxation coincides with the end-to-end relaxation (tube survival probability) in the absence of CR. Meanwhile, they also reported the retardation of the end-to-end relaxation due to the lack of CR. This finding contradicts to some tube theories, in which the tube survival probability (i.e., the end-to-end relaxation) is not

affected by CR. Indeed, in the well-developed tube model[20] and the single-chain slip-link model[21], CR does not affect the end-to-end relaxation. A possible theoretical explanation of this phenomenon is the CR-activated contour length fluctuations (CR-activated CLF) proposed by van Ruymbeke et al.[22,23]. They introduced the additional relaxation rate in the tube survival probability to incorporate the tension re-equilibration process induced by the CR-Rouse motion of the skinny tube in the dilated tube. Another possible idea has been proposed by Read et al[24,25] , who describe the effect of CR on the end-to-end relaxation by considering two different tubes for the constraints of short and long chains following the CR picture constructed by Viovy et al.[26]. Specifically, Read et al[24,25] suggest that the characteristic time of CR-activated CLF is dominated by sliding of the test chain along the skinny tube in its response to CR. Nevertheless, the probe rheology data with dielectric response has never been examined theoretically.

Apart from the significance of CR, there is the other multi-chain effect so-called orientational cross correlation (OCC). As mentioned above, the single chain models have achieved remarkable success on the basis of the assumption in which the

polymer chain moves independently. However, the experimental studies[27–29] have shown that there are cross-correlations between different chains. The cross correlation has been studied in molecular simulations as well. For instance, Cao and Likhtman[30] have reported that there exist considerable contributions of OCC in the relaxation modulus of polymer melts. They used Kremer-Grest type bead-spring simulations and measured the stress for each chain to extract the contribution of OCC. In their analysis, the OCC contribution increases in time, and it grows up to 40% of the total intensity at the terminal relaxation time. Similar results have been reported for multi-chain slip-link simulations[31,32]. In particular, Masubuchi and Amamoto[33] reported that the OCC contribution depends on the blend ratio and the short chain molecular weight for the case of bidisperse blends. This result suggests possible effects of OCC in the analysis of short chain signal in the probe rheology data.

In this study, multi-chain slip-link simulations were performed for the probe rheology data reported by Matsumiya et al.[19] The simulations reproduced the dielectric relaxation for the first time with the retardation due to the lack of CR. The coincidence between dielectric and viscoelastic relaxation spectrum for the probe chain

was also confirmed if shift-factors for the relaxation intensities are allowed. However, the simulated viscoelastic relaxations were not in good agreement for the relaxation intensity, possibly due to some flaws of OCC in the model. Details are shown below.

2 Model and Simulations

In the multi-chain slip-link simulations[34,35], polymers are represented by consecutive segments. Each segment carries a molecular weight comparable to the entanglement molecular weight. The segments are bundled via slip-links in pair to form a network in 3D space. The polymer motion is described by the Langevin-type equation of motion for the slip-link position and by the stochastic rate equation for the monomer transport through the slip-links. Both equations incorporate entropic elasticity of segment, osmotic force for segment density, friction with the medium, and thermal agitation. In addition, topological change of the network is considered via creation and destruction of slip-links at the chain ends. This topological change represents reptation of the test chain and CR for the partner chain.

To mimic the probe rheology experiment, the chain dynamics was examined in a gel network, in which the topological change of surrounding chains was suppressed.

The gels were obtained from equilibrated monodisperse melts by eliminating the creation and destruction of slip-links at the chain ends except for the probe chains. An important difference from probe rheology experiments is that the effect of CLF of the matrix chain is completely deactivated in the gels. Because the characteristic time of CLF is the Rouse time of the chain, the effect is not negligible if the matrix molecular weight is not sufficiently separated from that of probe chains. Indeed, Matsumiya et al[19] stated that for the longest probe chain with the molecular weight of 179k, the CLF dynamics of matrix chain with the molecular weight of 1.1M may affect it, although the Rouse time of the matrix chain is several times larger than the relaxation time of the probe chain (in the matrix). Nevertheless, due to the computational difficulties for the simulation with activated long chain matrices, the topologically frozen gels were employed as the matrix in this study.

The simulation code utilized in this study is identical to that used earlier for monodisperse and bidisperse[33,36,37] melts. The simulations were performed choosing the average equilibrium length of the segment a as unit length, kT as unit energy, $\tau_0 = \zeta a^2/6kT$ as unit time, where ζ is the friction coefficient of the slip-link. The unit

modulus is defined as $G_0 = \rho RT/M_0$, where M_0 is the average molar mass of the segment and ρ is polymer mass density[35,38].

Periodic boundary condition was employed with cubic simulation cells, for which the cell dimension was accommodated to be sufficiently larger than the chain dimensions (see Table I). Simulations under quiescent conditions were performed for sufficiently long times (10 times longer than the longest relaxation time for each case). For statistics, 16 independent runs with different initial configurations were performed for each case.

The linear relaxation modulus $G(t)$ was obtained from the auto-correlation function of shear stress. $G^*(\omega)$ was calculated from $G(t)$ via fitting to the multi-mode Maxwell relaxation function. The dielectric relaxation $\varepsilon^*(\omega)$ was obtained from the fluctuations of end-to-end vector. For both relaxations, auto-correlation for the same chain and cross-correlation between different chains were calculated from the data recorded for each chain. The entire relaxation and auto and cross-correlation contributions are denoted as $S(t)$, $A(t)$ and $C(t)$, respectively, with the subscripts S and P for segment orientation and end-to-end vector relaxations. The superscripts P and

M are for the probe and the matrix components. See Appendix A for the definition of the relaxation functions.

For polyisoprene (PI) data obtained by Matsumiya et al.[19], the parameters were determined as $M_0 = 3.5\text{k}$ and $\tau_0 = 4.5\times10^{-5}$ sec, to reproduce the data for monodisperse PI melts at 40℃ as shown in Figure 1. The unit modulus $G_0 = 6\times10^5\text{Pa}$ is determined from M_0. As reported earlier[35,38], the slip-link simulations reproduce the data semi-quantitatively, with the parameters shown above, although it is fair to note that the dielectric relaxation time for the shortest chain is apparently underestimated. The segment number per chain Z and the unit cell dimension L employed in the simulations are summarized in Table I.

Table I Segment number per chain Z and unit cell dimension L

M_w	Z	L
43k	12	10
99k	28	16
179k	51	20

For the probe rheology simulations, the probe chain fraction ϕ^P was fixed at 0.1 follwoing the experiment by Matsumiya et al. [19] It is noted however that they

employed $\phi^{\mathrm{P}} = 0.2$ for $M = 179\mathrm{k}$ due to the experimental convenience.

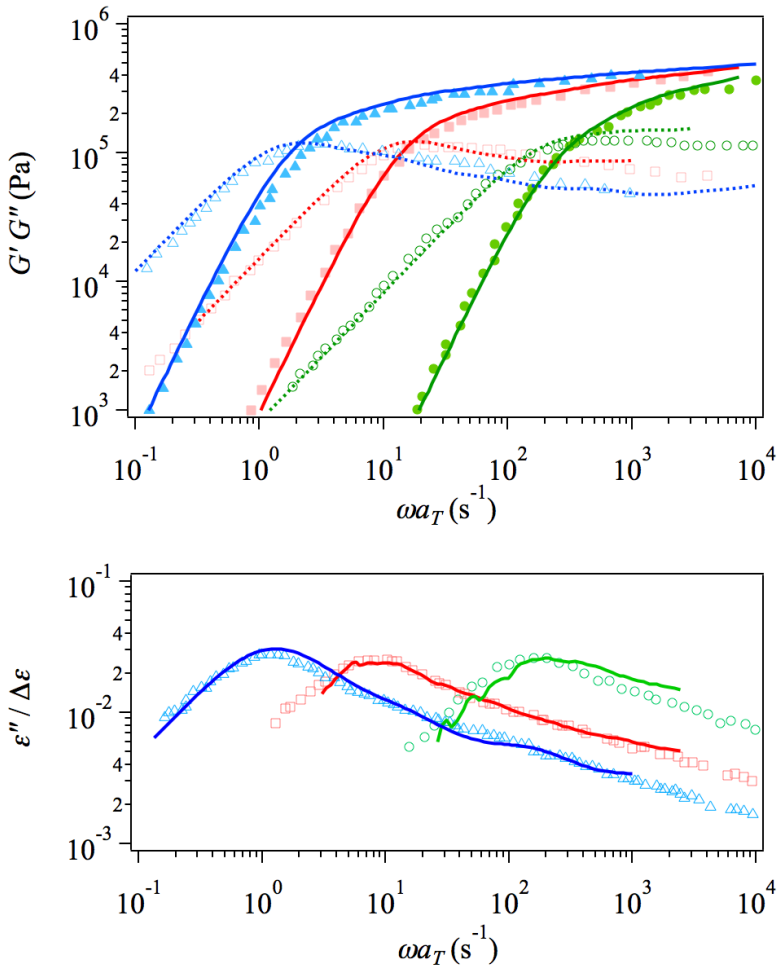

Figure 1 Linear viscoelasticity and dielectric loss for monodisperse PI melts at 40°C with the molecular weight of 179k (blue), 99k (red) and 43k (green) from left to right, respectively. Symbols are reproduced from Matsumiya et al.[19]. For the upper panel, filled and unfilled symbols are storage and loss moduli, respectively. Solid and dotted curves are storage and loss moduli from the simulations. For the bottom panel, the dielectric loss is shown with a similar manner to the viscoelasticity. Simulation parameters are described in the text.

3 Results and Discussion

3.1 Comparison to experimental data

Figure 2 shows the simulation results of loss modulus and dielectric loss for the probe chains in comparison to the experimental data[19]. The data for monodisperse melts are also shown for comparison. The simulation parameters for probe chains are identical to those used for the melts. The solid curves are obtained from $S_{\mathrm{S}}^{\mathrm{P}}(t)$ and $S_{\mathrm{P}}^{\mathrm{P}}(t)$ (see eq 8 in Appendix A). The simulation results are in reasonable agreement for the dielectric relaxation including the retardation of dielectric relaxation for the probe chain in comparison to the melt. In other words, $S_{\mathrm{P}}^{\mathrm{P}}(t)$ is affected by CR. This result contradicts a few theoretical predictions. Glomann et al.[20] argued that for the tube model proposed by Likhtman and McLeish[10], dielectric relaxation is insensitive to the inclusion of CR. Pilyugina et al.[21] reported similar results for the single-chain slip-link model. Nevertheless, the simulation is capable to predict the dielectric relaxations. The viscoelastic relaxation time is also reasonably captured according to the peak position for $G"(\omega)$ of the probes, $G"^{\mathrm{P}}(\omega)$. It is fair to note that the relaxation time for 43k is somewhat underestimated both for viscoelastic and dielectric relaxations but the discrepancy is consistent with that seen for the dielectric relaxation of the monodisperse

melt. On the other hand, the intensity of viscoelastic relaxation was not well-captured. Actually, in the experiment $G''^{\mathrm{P}}(\omega)$ is larger than $G''(\omega)$ for the monodisperse melts around the peak. For the simulations, the peak intensity of $G''^{\mathrm{P}}(\omega)$ is somewhat lower than $G''(\omega)$ for the melts. The intensity is virtually molecular weight independent for the experimental data whereas it decreases with decreasing molecular weight for the simulation.

It so appears that the simulation fails for the intensity of $G''^{\mathrm{P}}(\omega)$, and the failure suggests flaws in the simulations for CR and/or OCC. In the following sections, the effects of CR and OCC shall be analyzed in detail for end-to-end (dielectric) and segment (viscoelastic) relaxations.

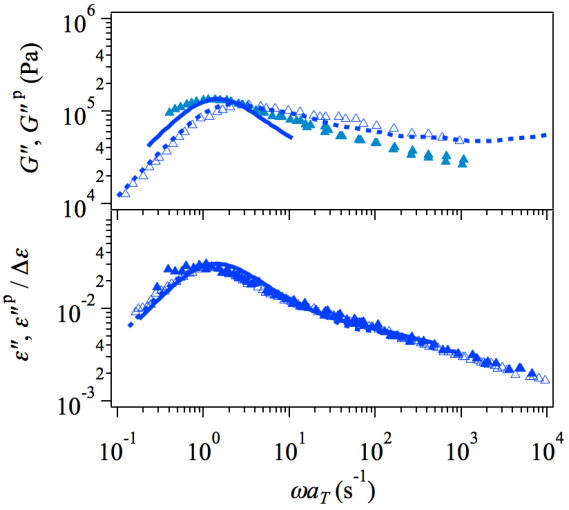

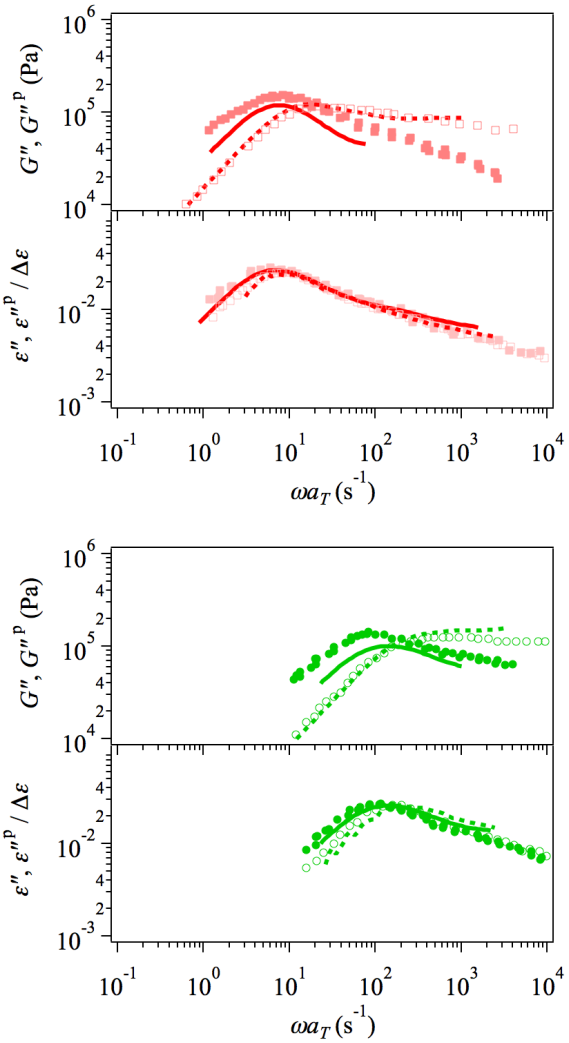

Figure 2 Loss modulus and dielectric loss of the probe chains in comparison to the monodisperse melts with the molecular weight of 179k (top), 99k (mid) and 43k (bottom). Symbols are the experimental data by Matsumiya et al.[19], and filled and unfilled ones represent the data for probe chains and for monodisperse melts, respectively. The probe chains are immersed in the matrix with the molecular weight of 1.1M in the experiment. Curves are the simulation results, in which solid ones are obtained from $S_{\mathrm{S}}^{\mathrm{P}}(t)$ and $S_{\mathrm{P}}^{\mathrm{P}}(t)$, and broken ones are for the monodisperse melts.

3.2 End-to-end relaxation

Figure 3 shows the end-to-end relaxation and its auto-correlation

contribution for probe chains and for melts. For melts, as reported earlier[31], $S_{\mathrm{P}}(t)$ and $A_{\mathrm{P}}(t)$ are not distinguishable from each other. This coincidence means that the cross-correlation is virtually negligible. The coincidence between $S_{\mathrm{P}}^{\mathrm{P}}(t)$ and $A_{\mathrm{P}}^{\mathrm{P}}(t)$ is observed for the probe chains as well. The other issue of interest is comparison between $S_{\mathrm{P}}^{\mathrm{P}}(t)$ of probe chains (solid curves) and $S_{\mathrm{P}}(t)$ in melts (broken curves), i.e., the effect of CR on the end-to-end relaxation. Namely, $S_{\mathrm{P}}^{\mathrm{P}}(t)$ is in retard of $S_{\mathrm{P}}(t)$, and the magnitude of retardation depends on the molecular weight. In particular, for the longest chain, there is almost no retardation. Our results are in good agreement with the data, as seen in Fig 2. The result seems in harmony with the idea of CR-activated CLF proposed by van Ruymbeke et al[22,23]. Actually, in the multi-chain slip-link simulations employed in this study, the effect of blinking slip-links propagates along the chain via the force balance. When a slip-link is created/destructed, the position of connected slip-links is changed due to the force balance, and a cascade of the position change of slip-links takes place along the chain. This argument might be also cast into the idea proposed by Read et al[24,25] if the wriggling of the chain is represented by the tube diameters, into which the effect of force balance is embedded. Nevertheless, the results for the

end-to-end relaxation suggest that the CR effects are reasonably implemented in the simulation.

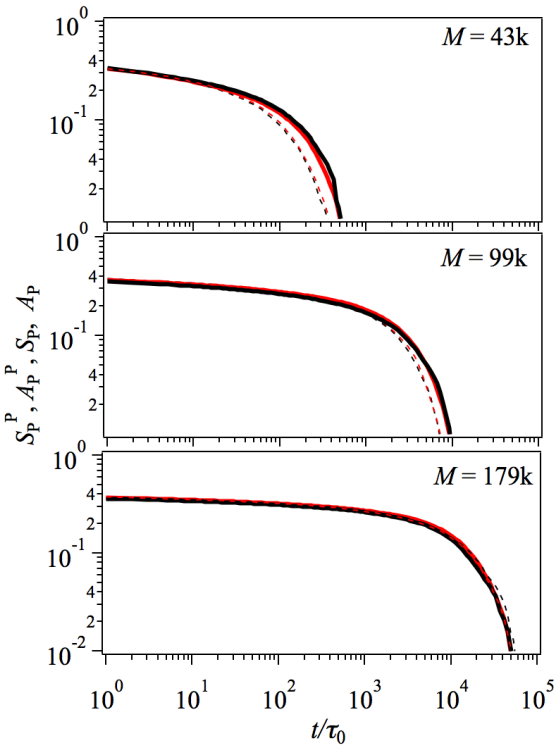

Figure 3 End-to-end relaxations for probe chains $S_P^P(t)$ and $A_P^P(t)$ (solid curves) and for monodisperse melts $S_P(t)$ and $A_P(t)$ (dotted curves). The molecular weight of PI is indicated in the figure. The entire relaxation ($S_P^P(t)$ and $S_P(t)$) and the auto-correlation contribution ($A_P^P(t)$ and $A_P(t)$) are indicated in black and red, respectively.

3.3 Segment relaxation

Figure 4 shows the segment correlation function for the probe chain $S_S^P(t)$

(black solid curve) plotted with $A_{\mathrm{S}}^{\mathrm{P}}(t)$ (red solid curve). Apparently, $A_{\mathrm{S}}^{\mathrm{P}}(t)$ is smaller than $S_{\mathrm{S}}^{\mathrm{P}}(t)$, indicating the effect of inter-chain cross-correlation. The cross-correlation contribution defined as $C_{\mathrm{S}}^{\mathrm{P}}(t) \equiv \phi^{\mathrm{P}} C_{\mathrm{S}}^{\mathrm{PP}}(t) + \phi^{\mathrm{M}} C_{\mathrm{S}}^{\mathrm{PM}}(t) \sim \phi^{\mathrm{M}} C_{\mathrm{S}}^{\mathrm{PM}}(t)$ are shown by green solid curves. $S_{\mathrm{s}}(t)$, $A_{\mathrm{s}}(t)$ and $C_{\mathrm{s}}(t)$ for monodisperse melts are shown by broken curves. For the relaxation rate, the probe chain relaxation is in retard of that in monodisperse melt due to the lack of CR, both for $A_{\mathrm{S}}^{\mathrm{P}}(t)$ and $C_{\mathrm{S}}^{\mathrm{P}}(t)$ (see the difference between solid and broken curves in red and green). $S_{\mathrm{S}}^{\mathrm{P}}(t)$ reflects these retarded relaxations, which are consistent with the experiment[19] as shown in Fig 2. On the other hand, the simulation failure for the intensity of $G''^{\mathrm{P}}(\omega)$ demonstrates flaws in the intensity of $S_{\mathrm{S}}^{\mathrm{P}}(t)$. Because the intensity of $A_{\mathrm{S}}^{\mathrm{P}}(t)$ is similar to that of $A_{\mathrm{s}}(t)$ and any reasonable mechanism to intensify $A_{\mathrm{S}}^{\mathrm{P}}(t)$ cannot be suggested, the simulation failure is due to the cross-correlation term $C_{\mathrm{S}}^{\mathrm{P}}(t)$. Indeed, $C_{\mathrm{S}}^{\mathrm{P}}(t)$ is smaller than $C_{\mathrm{s}}(t)$ for all the examined cases, and it contributes the intensity of $S_{\mathrm{S}}^{\mathrm{P}}(t)$. Note that however, $C_{\mathrm{S}}^{\mathrm{P}}(t)$ is mainly composed of the cross-correlation between probe and matrix chain $\phi^{\mathrm{M}} C_{\mathrm{S}}^{\mathrm{PM}}(t)$ (because of the condition at $\phi^{\mathrm{P}} = 0.1$), and thus, it is inherently different from $C_{\mathrm{s}}(t)$ in melts.

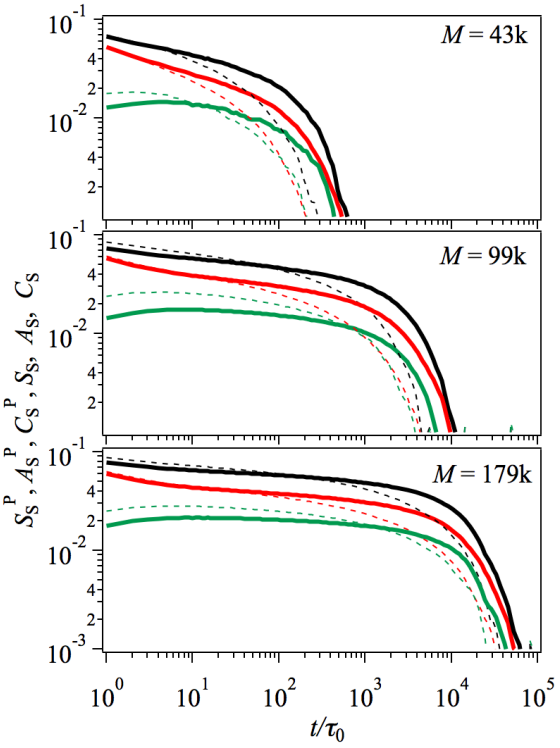

Figure 4 Correlation functions for segment orientation for probe chains (solid curves) and monodisperse melts (dotted curves). The molecular weight of PI is indicated in the figure. The entire function $S_s(t)$, the auto-correlation function $A_s(t)$ and the cross-correlation contribution $C_s(t)$ are indicated in black, red and green, respectively.

3.4 Comparison between end-to-end and segment relaxations

For further investigations, end-to-end and segment relaxations for the probe are compared with each other in this section. Watanabe[39] has shown that the end-to-end relaxation coincides with the segment relaxation given that the chain reptates in a fixed tube (without CR). To check this argument, Figure 5 shows the comparison among the

relaxation functions for the probe chain, $S_{\mathrm{S}}^{\mathrm{P}}(t)$, $S_{\mathrm{P}}^{\mathrm{P}}(t)$, $A_{\mathrm{S}}^{\mathrm{P}}(t)$ and $A_{\mathrm{P}}^{\mathrm{P}}(t)$. $S_{\mathrm{S}}^{\mathrm{P}}(t)$ and $A_{\mathrm{S}}^{\mathrm{P}}(t)$ are vertically shifted with appropriate shift-factors *a* and *b* to match $S_{\mathrm{P}}^{\mathrm{P}}(t)$ and $A_{\mathrm{P}}^{\mathrm{P}}(t)$. In the long-time region, in which the higher relaxation modes (e.g. Rouse modes) are not significant, all the relaxation functions coincide with each other. This result is in agreement with the data by Matsumiya et al.[19], who reported the coincidence for loss modulus and dielectric loss for the probe chains. (It is fair to note that in their data the relaxation functions do not coincide with each other for the probe chain with the molecular weight of 179k, because the probe molecular weight is not sufficiently different from the matrix molecular weight.) It is also noteworthy that $S_{\mathrm{S}}^{\mathrm{P}}(t)$ and $A_{\mathrm{S}}^{\mathrm{P}}(t)$ overlap with each other in the long-time region. This result indicates that the effect of $C_{\mathrm{S}}^{\mathrm{P}}(t)$ can be virtually replaced by the shift factor. In other words, $C_{\mathrm{S}}^{\mathrm{P}}(t)$ has virtually no effect on the longest relaxation time. This result lends support the discussion for the effect of CR on the relaxation time in the study by Matsumiya et al.[19] even though they did not consider the effects of cross-correlation.

The comparison among the relaxation functions shown above supports the discussion in the previous section for the failure in $G''^{\mathrm{P}}(\omega)$ in the simulation. Because

$S_{\mathrm{P}}^{\mathrm{P}}(t)$ is fully consistent with $\varepsilon''(\omega)$ that can be superposed to $G''^{\mathrm{P}}(\omega)$ in the experiment, the coincidence between $S_{\mathrm{S}}^{\mathrm{P}}(t)$ and $S_{\mathrm{P}}^{\mathrm{P}}(t)$ means that the relaxation time distribution of the segment relaxation is reasonably captured in the simulations. Namely, the shape and the horizontal location of $G''^{\mathrm{P}}(\omega)$is reasonably predicted in a similar extent to $\varepsilon''(\omega)$. The discrepancy is thus mainly in the intensity of $G''^{\mathrm{P}}(\omega)$, as discussed previously. Thus, it is reasonably concluded that $C_{\mathrm{S}}^{\mathrm{P}}(t)$ is the main reason of the failure in $G''^{\mathrm{P}}(\omega)$.

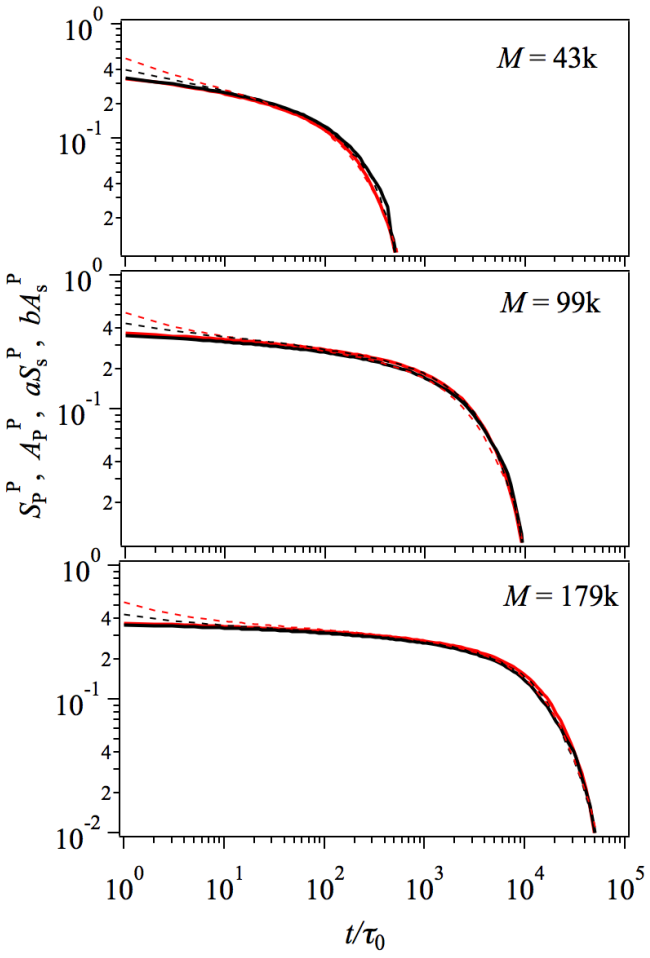

Figure 5 Comparison among the probe chain relaxation functions $S_S^P(t)$, $S_P^P(t)$, $A_S^P(t)$ and $A_P^P(t)$. Solid and dotted curves are end-to-end and segment relaxations, respectively. $S(t)$ and $A(t)$ are indicated in black and red.

4 Discussion

4.1 Problems in the present simulation

As mentioned in the previous section, the inconsistency for the viscoelastic data shown in Fig 2 is probably due to some flaws in OCC in the simulation. It is fair to

note that the employed model is not rigorous for the thermodynamic description[40]. In particular, the free energy expression of the system is unknown due to the osmotic force that suppress density fluctuations. The description of osmotic force may affect the present results. Actually, it has been reported that OCC is affected by the intensity of osmotic force[32]. In this respect, use of the other multi-chain models[41,42] constructed with rigorous thermodynamic expression is to be considered. Another possible flaw of the present study might be the use of gels rather than the actual long chain matrix. Even in the case in which the longest Rouse time of the matrix chain is well beyond the longest relaxation time of the probe chains, higher Rouse modes may affect the results. For these possibilities, although the computation cost is not practically affordable at this time being, further study is necessary.

4.2 Comparison to the tube theory

Owing to the fact that the tube models have attained quantitative agreement with melt data even neglecting OCC, one may argue that advanced tube models may be capable of describing the probe rheology data. In Figure 6, the prediction for probe

chain dynamics from the tube theory by Likhtman and McLeish[10] is shown by broken curves with the simulation results shown by thin solid curves. For the tube model, the CR intensity parameter c_ν is set at zero, and the other parameters were determined from the melt data as described in Appendix B. Note that the dielectric relaxation was obtained from the approximated analytical form given by eq 13 in the paper by Likhtman and McLeish[10], which is not in good agreement with the original stochastic simulations for the short chains. Thus, the result for *M*=43k chain may not be appropriate for further discussions.

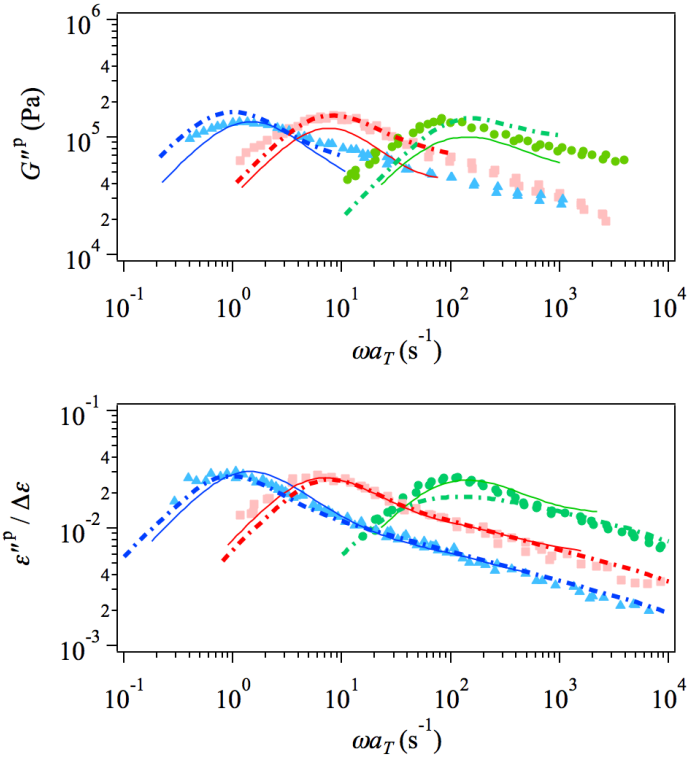

Figure 6 Loss modulus (top) and dielectric loss (bottom) of the probe chains with the molecular weight of 179k, 99k and 43k shown in blue, red and green, respectively.

Symbols are the experimental data by Matsumiya et al.[19]. Solid thin curves are the simulation results and identical to those shown in Figure 2. Broken curves are the prediction of Likhtman-McLeish model[10].

Figure 7 shows the dielectric relaxations for the monodisperse melts and for the probes with the tube prediction. Note that the dielectric relaxation is not affected by CR in the theory so that the tube prediction is identical for the monodisperse melt and the probe. Although the tube predictions for the long chains are in good agreement with the data for melts (as shown in Fig 10 in Appendix B), they deviate from the probe data, which exhibit the retardation from the melts.

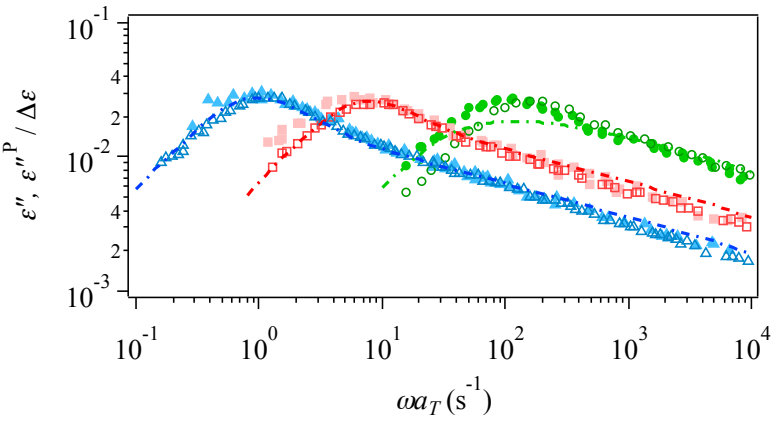

Figure 7 Dielectric relaxations of monodisperse melts and probes for M =179k, 99k and 43k shown in blue, red and green, respectively. Filled and unfilled symbols are for the probes and the monodisperse melts, respectively. Broken curves show the tube prediction[10].

Overall, the tube prediction is fairly good and the prediction accuracy is

comparable to that of the present simulation. For the dielectric relaxation (bottom panel), even though the tube prediction is insensitive to the lack of CR[20], the discrepancy with the experimental data is not large. For the viscoelastic relaxation, the relaxation intensity is in better agreement with the experiment than the simulation, although the relaxation time of the longest chain is somewhat overestimated.

As shown in Figure 6, two models are different for the description of the chain dynamics without CR. Figure 8 demonstrates the difference further explicitly for the longest chain with M =179k. In the top panel, curves in red are the prediction of $G(t)$ for the melt, and solid and broken curves are the simulation result and the tube prediction, respectively. Note that for the tube model the c_v parameter is chosen at 1.0 for the melt case, as determined in Appendix B. These two results are in good agreement with experiment (as shown in Figs 1 and 10 by blue curves, the latter is in Appendix B). In the bottom panel, the tube survival probability $\mu(t)$ is shown. Because $\mu(t)$ is the segment relaxation function for the test chain in a fixed tube, the counterpart in the simulation is assumed to be $A_S^P(t)$, which is also shown for comparison. Due to the cross-correlation contributions (as discussed for Fig 4), the

relaxation intensity of $A_S^P(t)$ is smaller than that of $\mu(t)$. To accommodate the difference in relaxation intensity, $A_S^P(t)$ is vertically shifted and shown by dotted curve in red in the bottom panel. The comparison demonstrates that $A_S^P(t)$ relaxes faster than $\mu(t)$. These differences between $A_S^P(t)$ and $\mu(t)$ are concealed in $G(t)$ by the different implementations of CR dynamics, and by the cross-correlation.

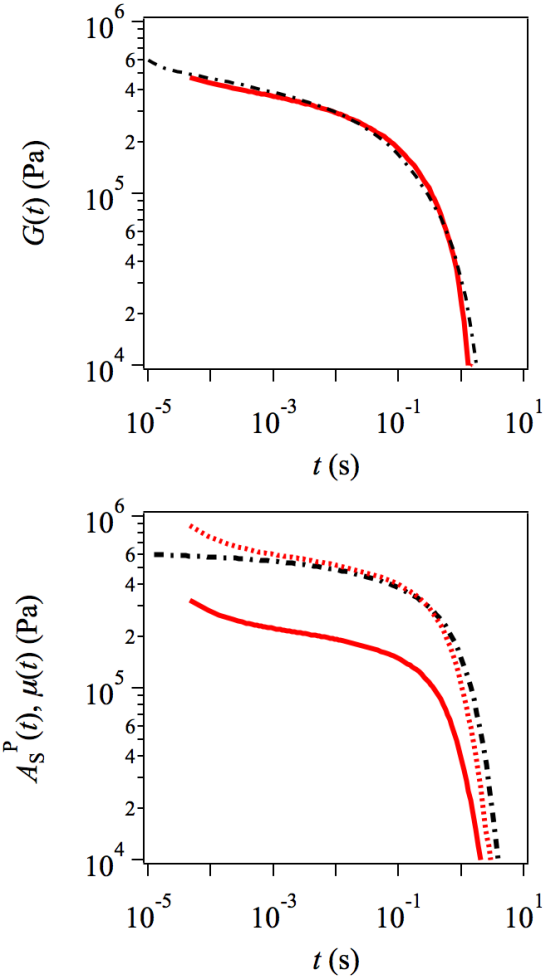

Figure 8 Linear relaxation modulus $G(t)$ (top) and tube survival function $\mu(t)$ (bottom) for the melt of M =179k from the simulation (red solid curves) and the tube theory (black broken curves). In the bottom panel $A_S^P(t)$ from the simulation is shown for comparison to $\mu(t)$ in the tube theory[10]. Red dotted curve is $A_S^P(t)$ with a vertical shift.

It is fair to note that, as mentioned earlier, there are further advanced tube models[23–25], which take account of the effects of CR on the end-to-end relaxation. In particular, Shivokhin et al.[25] have proposed the expression of the end-to-end relaxation time for the chains placed in various CR environments. Their theory is actually applicable to the probe rheology, even though their study rather focused CR conditions in which the CR relaxation time is faster than the reptation time of the test chain. However, the magnitude of accerelation for the end-to-end relaxation due to CR depends on the phenomenological parameter in the crossover function between different CR regimes, so that detiled discussion seems difficult. Indeed, Shivokhin et al.[25] restricted themselves to the qualitative discussion about the comparison to the data by Matsumiya et al.[19] Nevertheless, the effect of CR on the end-to-end relaxation is a challenge for the single chain models.

4 Conclusions

The probe rheology data reported by Matsumita et al.[19] were examined via primitive chain network simulations. The retardation in dielectric relaxation due to the

lack of CR was captured, and consequently, the dielectric relaxation was semi-quantitatively reproduced. This result is conceptually in harmony with the CR-accelerated CLF[22,23]. On the other hand, the viscoelastic relaxation was not in good agreement with the experimental data, for the relaxation intensity in particular. The source of discrepancy was analyzed in terms of the cross-correlation between the probe chains and the matrix chains for the relaxations of end-to-end vector and the segment orientation. For the end-to-end relaxation, the cross-correlation is virtually negligible, whereas for the segment relaxation, it has a considerable contribution in the total relaxation modulus. Even with such a difference in the cross-correlation contribution, the end-to-end and segment relaxations are superposable with a certain shift-factor for the intensity, being fully consistent with the experimental result. The coincidence between end-to-end and segment relaxations demonstrates that the relaxation time and its distribution are reasonably reproduced even for the viscoelastic relaxation. On the other hand, the intensity of viscoelastic relaxation is underestimated due to the failure of the simulation in the cross-correlation contribution. The failure might be due to the flaw of the model that is not thermodynamically rigorous, and due to the use of gel for the

matrix rather than the actual mobile long chain.

It so appears that the probe rheology with viscoelastic and dielectric measurements is quite useful for the test of molecular models. Indeed, the difference between the simulation and the tube model is exhibited in the probe rheology predictions whereas it is concealed in the viscoelasticity of monodisperse melts. For the comparison, the dielectric data are important to fix the parameters. Even though there are lots of attempts for the probe rheology, the dielectric relaxation has not been frequently discussed. Further studies from experimental and theoretical sides are of necessity.

Conflicts of interest

There are no conflicts of interest to declare.

Acknowledgements

The authors thank Prof. Hiroshi Watanabe, Kyoto University, for his useful comments. This work is supported in part by Grant-in-Aid for Scientific Research (A) (17H01152)

from JSPS and by Council for Science, Technology and Innovation, Cross-ministerial Strategic Innovation Promotion Program, “Structural Materials for Innovation” from JST.

Appendix A: Correlation Functions

In this section, the correlation functions to be discussed in the text are summarized. Because the analysis has been proposed earlier by Cao and Likhtman[30], readers familiar with their study may skip this section.

Owing to the fluctuation dissipation theorem, the linear relaxation modulus $G(t)$ can be obtained from the segment orientational correlation function $S_{\mathrm{s}}(t)$ with the stress-optical coefficient α.

$$G(t) = \frac{1}{\alpha} S_{\mathrm{s}}(t) \tag{1}$$

Here, $S_{\mathrm{s}}(t)$ is defined as,

$$S_{\mathrm{s}}(t) \equiv N_{\mathrm{b}} \left(\frac{1}{N_{\mathrm{b}}} \sum_{J=1}^{N_{\mathrm{c}}} O_J^{xy}(t) \right) \left(\frac{1}{N_{\mathrm{b}}} \sum_{J=1}^{N_{\mathrm{c}}} O_J^{xy}(0) \right) \tag{2}$$

Here, N_{b} is the total number of segments and N_{c} the number of chains in the system. The segment orientation tensor O_J^{xy} is defined as,

$$O_J^{xy}(t) \equiv \sum_{i=1}^{Z_J} \frac{r_{iJ}^x(t) r_{iJ}^y(t)}{n_{iJ}(t)} \qquad (3)$$

Here, Z_J is the number of segments for chain J, and $n_{iJ}(t)$ and $\mathbf{r}_{iJ} = \left(r_{iJ}^x, r_{iJ}^y, r_{iJ}^z\right)$ are the Kuhn segment number and the end-to-end vector for segment i on chain J, respectively. Note that the Kuhn segment number $n_{iJ}(t)$ is normalized by n_0 that is the average number of Kuhn segments on one entanglement segment carrying the unit molecular weight M_0.

For a system containing matrix and probe chain components, $S_\mathrm{s}(t)$ can be decomposed as,

$$S_\mathrm{s}(t) = \phi^\mathrm{M} A_\mathrm{S}^\mathrm{M}(t) + {\phi^\mathrm{M}}^2 C_\mathrm{S}^\mathrm{MM}(t) + \phi^\mathrm{P} A_\mathrm{S}^\mathrm{P}(t) + {\phi^\mathrm{P}}^2 C_\mathrm{S}^\mathrm{PP}(t) + 2\phi^\mathrm{M}\phi^\mathrm{P} C_\mathrm{S}^\mathrm{MP}(t) \quad (4)$$

A_S^A and C_S^AB are auto and cross correlations defined as,

$$A_\mathrm{S}^\mathrm{A}(t) = N_\mathrm{b} \frac{1}{\phi^\mathrm{A} {N_\mathrm{b}}^2} \sum_{J \in \mathrm{A}} O_J^{xy}(t) O_J^{xy}(0) \qquad (5)$$

$$C_\mathrm{S}^\mathrm{AB}(t) = N_\mathrm{b} \frac{1}{\phi^\mathrm{A}\phi^\mathrm{B} {N_\mathrm{b}}^2} \sum_{I \in \mathrm{A}, J \in \mathrm{B}} \sum_{I \neq J} O_I^{xy}(t) O_J^{xy}(0) \quad (6)$$

The superscripts A and B stand for the matrix (M) or probe (P) components.

Equation 4 can be rewritten as the sum of the contributions from the matrix and the probe chain components,

$$S_{\mathrm{s}}(t) = \phi^{\mathrm{M}} S_{\mathrm{S}}^{\mathrm{M}}(t) + \phi^{\mathrm{P}} S_{\mathrm{S}}^{\mathrm{P}}(t) \qquad (7)$$

Note that the contribution from each component includes the cross-correlation terms;

$$S_{\mathrm{s}}^{\mathrm{A}}(t) = A_{\mathrm{S}}^{\mathrm{A}}(t) + \phi^{\mathrm{A}} C_{\mathrm{S}}^{\mathrm{AA}}(t) + \phi^{\mathrm{B}} C_{\mathrm{S}}^{\mathrm{AB}}(t) \qquad (8)$$

The relaxation modulus for component A, $G^{\mathrm{A}}(t)$, can be obtained from $S_{\mathrm{s}}^{\mathrm{A}}(t)$ with the stress-optical coefficient α as $G^{\mathrm{A}}(t) = S_{\mathrm{s}}^{\mathrm{A}}(t)/\alpha$.

In a similar manner to the segment orientation, the relaxation can be defined for the end-to-end vector as follows,

$$S_{\mathrm{P}}(t) \equiv N_{\mathrm{c}} \left(\frac{1}{N_{\mathrm{c}}} \sum_{J=1}^{N_{\mathrm{c}}} P_J^x(t) \right) \left(\frac{1}{N_{\mathrm{c}}} \sum_{J=1}^{N_{\mathrm{c}}} P_J^x(0) \right) \qquad (9)$$

$$P_J^x(t) = \sum_{i=1}^{Z_{\mathrm{J}}} r_{iJ}^x(t) \Big/ \sum_{i=1}^{Z_{\mathrm{J}}} n_{iJ}(t) \qquad (10)$$

$S_{\mathrm{P}}(t)$ is proportional to the dielectric relaxation function of type-A polymers. The auto and cross-correlation functions, $A_{\mathrm{P}}(t)$ and $C_{\mathrm{P}}(t)$, and the contribution from each component are defined as of eqs 5-8.

Appendix B: Determination of parameters for the tube model

For the comparisons shown in Figs 6-8, the parameters for the tube model[10]

were determined as described here. The model parameters are the unit of molecular weight, modulus and time, and the CR intensity parameter, which are denoted as M_0^{LM}, G_0^{LM}, τ_0^{LM} and c_ν, respectively. The value of M_0^{LM} was chosen at $M_0^{\mathrm{LM}} = 4820$ according to the literature by Auhl et al.[43]. G_0^{LM} was chosen at $G_0^{\mathrm{LM}} = 0.624$ GPa, which is modified from the value reported by Auhl et al.[43] due to the difference of temperature (G_0^{LM} reported by Auhl et al.[43] is 0.595 GPa for 25℃, whereas the temperature for the data by Matsumiya et al. is 40℃). The other parameters were determined via the fitting to the melt data for M =179k. Owing to the nature of dielectric relaxation that is not affected by c_ν, τ_0^{LM} was firstly determined from the fitting of dielectric loss data as $\tau_0^{\mathrm{LM}} = 1.25 \times 10^{-5}$sec. Afterwards, c_ν was determined to attain the best fit to the viscoelastic data. Figure 9 shows the comparison to the experimental data with various c_ν values and the other parameter values mentioned above. The top panel demonstrates significant effects of c_ν on the viscoelastic relaxation. Auhl et al.[43] suggested $c_\nu = 0.1$ but with this value the viscoelastic relaxation time is largely overestimated (see red curves) given that τ_0^{LM} is fixed by the fitting to the dielectric relaxation. Indeed, Auhl et al.[43] did not discuss the dielectric

relaxation to determine their c_v value. Nevertheless, Fig 9 clearly demonstrates that $c_v = 1.0$ gives the best fit for this specific case. Owing to the result, the melt calculations were made for the other molecular weights with the same parameter set as shown in Fig 10. For the shorter chains (M=99k and 43k shown in red and green), the tube theory underestimates the viscoelastic relaxation time. This discrepancy may not appear if c_v is tuned for each molecular weight, as reported by Glomann et al.[20]. Indeed, for M=99k case, since the dielectric loss is excellently predicted, the viscoelastic relaxation would be better predicted with a smaller c_v value. For the shortest chain (M=43k) the dielectric relaxation is not correctly described due to the use of the approximated function (eq 13 in the paper by Likhtman and McLeish[10]), which is not in good agreement with the results obtained from the stochastic simulations for short chains (see the paper by Likhtman and McLeish[10]). Nevertheless, the results from the tube model shown in Figs 6 - 8 were made with the parameters given above, except the c_v parameter that is set to zero to suppress CR for the case of probe chains.

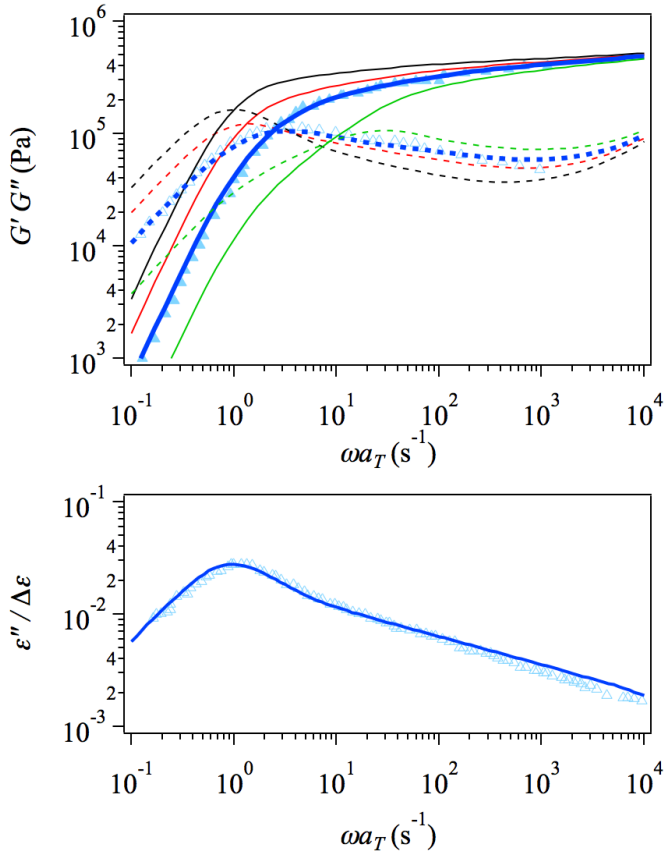

Figure 9 Prediction of the tube theory[10] for viscoelastic (top) and dielectric (bottom) relaxations of the monodisperse melt for M =179k. The prediction and the experimental results are shown by curves and symbols, respectively. The parameters are $M_0^{\mathrm{LM}} = 4820$, $G_0^{\mathrm{LM}} = 0.624$ GPa and $\tau_0^{\mathrm{LM}} = 1.25 \times 10^{-5}$sec. c_ν was varied as 0, 0.1, 1.0 and 10, and the results are shown by the curves in black, red, blue and green, respectively. Storage and loss moduli are shown by solid and dotted curves. The experimental data were reported by Matsumiya et al.[19]

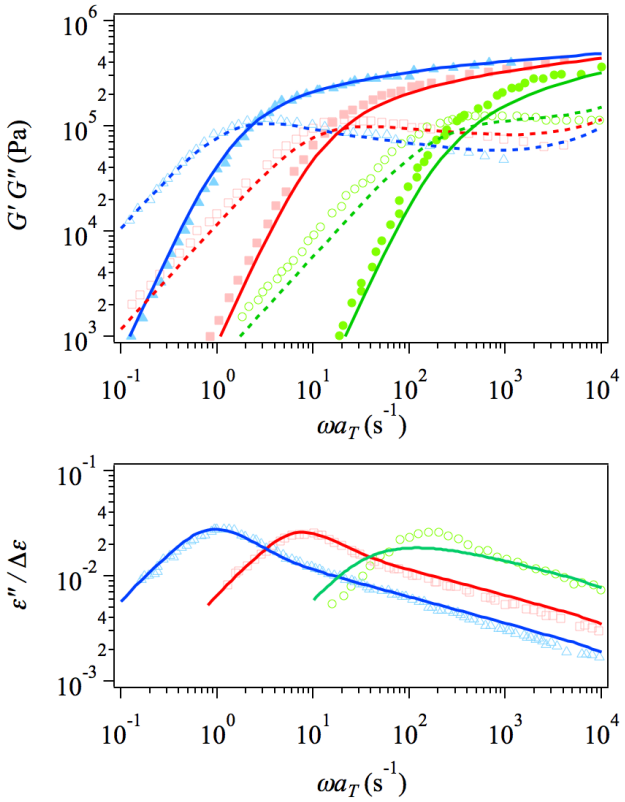

Figure 10 Prediction of the tube theory[10] for viscoelastic (top) and dielectric (bottom) relaxations of monodisperse PI melts for M =179k, 99k and 43k shown in blue, red and green, respectively. Predictions and experimental results are shown by curves and symbols, respectively. The experimental data were reported by Matsumiya et al.[19]

REFERENCES

1 Y. Masubuchi, *Annu. Rev. Chem. Biomol. Eng.*, 2014, **5**, 11–33.

2 Y. Masubuchi, in *Reference Module in Materials Science and Materials Engineering*, Elsevier, 2016, pp. 1–7.

3 H. Janeschitz-Kriegl, *Fortschritte der Hochpolym.*, 1969, **6/2**, 170–318.

4 J. D. Ferry, *Viscoelastic Properties of Polymers*, John Wiley & Sons, Inc., 3rd edn., 1980.

5 P. E. Rouse, *J. Chem. Phys.*, 1953, **21**, 1272.

6 S. F. Edwards, *Proc. Phys. Soc.*, 1967, **92**, 9–16.

7 P. G. de Gennes, *J. Chem. Phys.*, 1971, **55**, 572.

8 M. Doi and S. F. Edwards, *The Theory of Polymer Dynamics*, Clarendon press, Oxford, 1986.

9 S. T. Milner and T. C. B. McLeish, *Phys. Rev. Lett.*, 1998, **81**, 725–728.

10 A. E. Likhtman and T. C. B. McLeish, *Macromolecules*, 2002, **35**, 6332–6343.

11 M. Doi and S. F. Edwards, *J. Chem. Soc. Faraday Trans. 2*, 1978, **74**, 1789.

12 M. Doi, *J. Polym. Sci. Polym. Phys. Ed.*, 1983, **21**, 667–684.

13 W. W. W. Graessley, in *ADVANCES IN POLYMER SCIENCE*, Springer-Verlag, Berlin/Heidelberg, 1982, vol. 47, pp. 67–117.

14 C. Tsenoglou, *ACS Polym. Prepr.*, 1987, **28**, 185–186.

15 J. des Cloizeaux, *Europhys. Lett.*, 1988, **5**, 437–442.

16 G. Marrucci, *J. Polym. Sci. Polym. Phys. Ed.*, 1985, **23**, 159–177.

17 H. Watanabe, *Prog. Polym. Sci.*, 1999, **24**, 1253–1403.

18 C. Liu, A. F. Halasa, R. Keunings and C. Bailly, *Macromolecules*, 2006, **39**, 7415–7424.

19 Y. Matsumiya, K. Kumazawa, M. Nagao, O. Urakawa and H. Watanabe, *Macromolecules*, 2013, **46**, 6067–6080.

20 T. Glomann, G. J. Schneider, A. R. Bras, W. Pyckhout-Hintzen, A. Wischnewski, R. Zorn, J. Allgaier and D. Richter, *Macromolecules*, 2011, **44**, 7430–7437.

21 E. Pilyugina, M. Andreev and J. D. Schieber, *Macromolecules*, 2012, **45**, 5728–5743.

22 E. van Ruymbeke, Y. Masubuchi and H. Watanabe, *Macromolecules*, 2012, **45**, 2085–2098.

23 E. Van Ruymbeke, V. Shchetnikava, Y. Matsumiya and H. Watanabe, *Macromolecules*, 2014, **47**, 7653–7665.

24 D. J. Read, K. Jagannathan, S. K. Sukumaran and D. W. Auhl, *J. Rheol. (N. Y. N. Y).*, 2012, **56**, 823.

25 M. E. Shivokhin, D. J. Read, D. Kouloumasis, R. Kocen, F. Zhuge, C. Bailly, N.

Hadjichristidis and A. E. Likhtman, *Macromolecules*, 2017, **50**, 4501–4523.

26 J. L. Viovy, M. Rubinstein and R. H. Colby, *Macromolecules*, 1991, **24**, 3587–3596.

27 R. Graf, A. Heuer and H. W. Spiess, *Phys. Rev. Lett.*, 1998, **80**, 5738–5741.

28 J. a Kornfield, G. G. Fuller and D. S. Pearson, *Macromolecules*, 1989, **22**, 1334–1345.

29 C. M. Ylitalo, J. a Kornfield, G. G. Fuller and D. S. Pearson, *Macromolecules*, 1991, **24**, 749–758.

30 J. Cao and A. E. Likhtman, *Phys. Rev. Lett.*, 2010, **104**, 207801.

31 Y. Masubuchi and S. K. Sukumaran, *Nihon Reoroji Gakkaishi*, 2013, **41**, 1–6.

32 Y. Masubuchi and Y. Amamoto, *Nihon Reoroji Gakkaishi*, 2016, **44**, 219–222.

33 Y. Masubuchi and Y. Amamoto, *Macromolecules*, 2016, **49**, 9258–9265.

34 Y. Masubuchi, J.-I. I. Takimoto, K. Koyama, G. Ianniruberto, G. Marrucci and F. Greco, *J. Chem. Phys.*, 2001, **115**, 4387.

35 Y. Masubuchi, G. Ianniruberto, F. Greco and G. Marrucci, *J. Chem. Phys.*, 2003, **119**, 6925–6930.

36 Y. Masubuchi, H. Watanabe, G. Ianniruberto, F. Greco and G. Marrucci, *Macromolecules*, 2008, **41**, 8275–8280.

37 K. Takeda, S. K. Sukumaran, M. Sugimoto, K. Koyama and Y. Masubuchi, *Adv. Model. Simul. Eng. Sci.*, 2015, **2**, 11.

38 Y. Masubuchi, G. Ianniruberto, F. Greco and G. Marrucci, *J. Nonnewton. Fluid Mech.*, 2008, **149**, 87–92.

39 H. Watanabe, *Macromol. Rapid Commun.*, 2001, **22**, 127–175.

40 T. Uneyama and Y. Masubuchi, *J. Chem. Phys.*, 2011, **135**, 184904.

41 V. C. Chappa, D. C. Morse, A. Zippelius and M. Müller, *Phys. Rev. Lett.*, 2012, **109**, 148302.

42 T. Uneyama and Y. Masubuchi, *J. Chem. Phys.*, 2012, **137**, 154902.

43 D. Auhl, J. Ramirez, A. E. Likhtman, P. Chambon and C. Fernyhough, *J. Rheol. (N. Y. N. Y).*, 2008, **52**, 801.